Nuclear Materials and Energy 38 (2024) 101625

Contents lists available at ScienceDirect

Nuclear Materials and Energy

journal homepage: www.elsevier.com/locate/nme

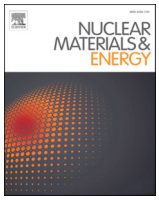

HICU PIE results of neutron-irradiated lithium metatitanate pebbles

Julia Leys *, Rolf Rolli, Hans-Christian Schneider, Regina Knitter

Karlsruhe Institute of Technology (KIT), Institute for Applied Materials (IAM), 70621 Karlsruhe, Germany

ARTICLE INFO

Keywords:
Fusion technology
Ceramic tritium breeder
Lithium metatitanate
HICU experiment
Neutron irradiation
Post-irradiation examination

ABSTRACT

Lithium metatitanate (Li_2TiO_3) pebbles were irradiated with neutrons within the HICU (High neutron fluence Irradiation of pebble staCks for fUsion) experiment to investigate their material properties and tritium release behaviour in a post-irradiation examination (PIE). The irradiation temperature is the most significant influence on the material. Besides a higher irradiation temperature, a higher initial Li–6 content tends to lead to an increased tritium generation resulting in the formation of the secondary lithium depleted phase $Li_4Ti_5O_{12}$. A pre-compaction of the pebble bed does not have an apparent influence on the material properties. Tritium is released as semi-tritiated water and semi-tritiated hydrogen (HTO and HT) and its release is enhanced at elevated irradiation temperatures.

1. Introduction

Lithium metatitanate is one of the candidate materials to be used as a tritium breeder material in future fusion reactors. Beside standard characterisations of the ceramic material, it is essential to test it under fusion relevant conditions, in particular the irradiation with neutrons. Therefore, the HICU experiment was performed for lithium ceramic materials in the High Flux Reactor (HFR) in Petten, Netherlands [1]. Besides lithium silicate pebbles (Li_4SiO_4 incl. ~10 mol% Li_2SiO_3) supplied by *Karlsruhe Institute of Technology* (KIT, former FZK), Germany, lithium metatitanate pebbles (Li_2TiO_3) supplied by *National Institute for Quantum Science and Technology* (QST; former JAEA), Japan, and by *Commissariat à l'énergie atomique et aux énergies alternatives* (CEA), France, were included in the HICU experiment. Among the samples provided by each supplier, their initial Li–6 content differed. Some pebble beds were pre-compacted before the irradiation and there were two different temperature zones within the irradiation experiment. The irradiation campaign took place between early 2008 and the end of 2010. The HICU experiment should address DEMO-relevant conditions. A shielding of the samples was used to adapt the neutron spectrum in the reactor. Damage levels were aimed at 20–25 dpa (in the ceramics). While the PIE of lithium silicate pebbles was already published [2,3], this study focuses on the PIE of the Li_2TiO_3 pebbles provided by CEA. A direct comparison between irradiated and pristine (unirradiated) samples can only be made for some material properties due to a lack of data available for the pristine pebbles.

2. Material and methods

2.1. Examined irradiated samples

For the HICU experiment, eight different batches of Li_2TiO_3 pebbles were provided by CEA. The pebbles were fabricated using the extrusion-spheronisation sintering process in collaboration with the *Commission des Titres d'Ingénieur* (CTI), France [4]. The supplied pebble samples differed in their Li–6 contents as follows: Li–6 depletion (0.06 at%), natural abundance (7.5 at%), moderate (11 at%) and high Li–6 enrichment (30 at%).

The pebble samples experienced different temperatures during the irradiation. They were irradiated at a lower temperature of about 650 °C and in a higher temperature range of about 800–850 °C. In the following, these different irradiation conditions are referred to as *low temperature* (LT) and *high temperature* (HT).

Moreover, some pebble beds were pre-compacted while others were not. Therefore, some samples experienced a low strain (no initially applied stress) and some a high strain (pebble beds were pre-compacted at 0.7 MPa). In the following, both states are referred to as *low constraint* (LC) and *high constraint* (HC). For samples that were irradiated under HC, different capsule types with a larger diameter were used. Hence, higher sample amounts were irradiated.

For the PIE of the HICU experiment, 10 out of 21 of the irradiated Li_2TiO_3 pebble samples were selected. These samples allow the investigation of influences resulting from the Li–6 content, the irradiation temperature and different constraints of the pebble beds. Samples with

* Corresponding author.
E-mail address: julia.leys@kit.edu (J. Leys).

https://doi.org/10.1016/j.nme.2024.101625
Received 14 December 2023; Received in revised form 21 February 2024; Accepted 26 February 2024
Available online 1 March 2024

natural Li–6 abundance result from three different batches, while the other Li–6 contents result in each case from only one batch. All 10 samples included in the PIE and their initial sample properties determined by CEA and the *Nuclear Research and Consultancy Group* (NRG) are summarised in Table 1. CEA provided porosity values, which were used to determine a "CEA density" considering a theoretical density (*TD*) of 3.415 g/cm^3 for Li_2TiO_3 [5]. Density values measured by NRG using helium pycnometry differ slightly from those [6]. From the "NRG density" another set of closed porosity values was determined. For comparison of the results obtained within the HICU PIE and the properties of the pristine pebbles, average values from CEA and NRG listed in Table 1 are considered.

The samples were irradiated within 15 cycles of about 29 days while purged with helium with additions of 0.1 % hydrogen. The samples reached damage levels of about 6, 10 or 15 dpa (see Table 1) [7]. The lithium burn-up was only calculated for a few samples of the whole campaign. For sample HT–30–LC included in the presented PIE a lithium burn-up of 5.6 % was calculated (the sample holder was located in the centre of the rig, closest to the flux axial peak position) [7]. The neutron spectrum was adapted using a cadmium shielding to cut off the thermal neutrons and to achieve DEMO relevant conditions.

2.2. Characterisation techniques

Before the HICU PIE, the irradiated samples were retrieved from the capsules. At times the use of mechanical force could not be avoided as pebbles stuck to the walls of the capsules. The pebble samples were then sieved to remove any generated dust.

Within the PIE, powder X-ray diffraction (XRD) was used to analyse the phase content of the ceramic pebbles. A silicon wafer was used as sample holder due to the small sample amounts. For each sample, a small amount was ground in an agate mortar. From this powder, three individual measurements were performed. XRD patterns were recorded within the 2-theta range of 10–120° using a D2 PHASER (Bruker AXS) equipped with a Cu Kα source (stepwidth: 0.02°, time per step: 3 s, rotation: 15 rpm). In addition, a selected sample was measured by XRD before and after an oxidation in synthetic air (700 °C, 5 h). Qualitative phase analysis was performed using EVA Software (Bruker AXS). Rietveld refinements were done in Topas–6 (Bruker AXS) based on the crystallographic information files (CIF) by Kataoka et al. [5] for Li_2TiO_3 and by Li et al. [8] for $Li_4Ti_5O_{12}$. The resulting data was averaged from the refinements of the aforementioned three diffraction patterns per sample.

Optical micrographs were taken using an optical inverted Olympus GX51 Light Optical Microscope equipped with an HR CCD camera. The dimensions were measured from a monolayer of pebbles. About ten pebbles of each sample were embedded in epoxy resin, ground to almost their centres and then polished with liquid paraffin.

Microstructural analyses by scanning electron microscopy (SEM) were carried out using a 40 kV RemX/Cam Scan 44 equipped with an energy-dispersive X-ray spectroscopy (EDS) analyser. Cross sections, prepared as described above, and the surfaces of whole pebbles were investigated. To mitigate charging effects, all samples were sputtered with platinum.

The closed porosity of the Li_2TiO_3 pebbles after irradiation was determined on the basis of density measurements using helium pycnometry (Quantachrome: multipycnometer, MVP–1). For each sample, masses between 0.5 and 2 g were used for five repetitive measurements.

The mechanical strength of individual pebbles was determined by the uniaxial compression of the pebbles until their failure. Crush load tests were performed using a Zwick Precision Line Vario instrument (BK7 glass plates) within a glove box with a nitrogen atmosphere for 40 pebbles per irradiated sample. As far as possible, pebbles of uniform size were selected. For all but two samples, a pebble diameter of about 1 mm (σ = 0.04) was used. The provided size range of the two samples LT–7.5–HC and LT–7.5–LC_b was smaller; hence crush load tests were performed with diameters of about 0.7 mm in this case. Prior to the actual testing, the pebbles were heated up to 300 °C for one hour in a vacuum.

The tritium release behaviour of the irradiated Li_2TiO_3 pebbles was recorded in thermally programmed desorption (TPD) experiments. About 0.02 g of each sample were heated up to 1100 °C with a heating rate of 7 K/min. After a dwell time of 3 h at the maximum temperature the pebble samples were cooled down to room temperature with a cooling rate of 10 K/min. The reference purge gas He + 0.1 % H_2 was used to transport the released gas species to a quadrupole mass spectrometer (QMS) by MKS Instruments (Process Eye). Subsequently, the gas was led through a Zn-bed operating at 370 °C to reduce the occurring tritiated water to a hydrogen isotopologue. After that, the gas stream was led into an ionisation chamber (IC) for monitoring. The IC has a volume of 100 ml and a time resolution of 30 s. To prevent condensation all gas piping was held at 250 °C during the experiments. The IC was used to detect the activity resulting from the released tritium. The recorded TPD curves were multiplied by a correction factor. This correction factor was determined using a calibration gas. As the availability of certified tritium gas is very low, an uncertified gas was used for the calibration. This gas has a maximum tritium content deviation of 5 %, which was considered as acceptable.

3. Results and discussion

3.1. Visual inspection and geometrical characterisation

All samples exhibit a change in colour after the neutron irradiation

Table 1
Properties provided for the pristine (unirradiated) Li_2TiO_3 pebble samples (determined by CEA and NRG). Furthermore, their temperature (high = ~800–850 °C / low = ~650 °C) and their constraint (high = 0.7 MPa pre-load / low = no pre-load) during the irradiation and the achieved dpa (calculated) is given. In the following, the sample names are composed by the first three columns of this table.

T_{irr} /°C	Initial Li-6 content / %	Constraint	Sample name	Batch	Exp. weight / g	Pebble size (CEA) / mm	ρ (NRG) / g/cm^3	Closed porosity (CEA) / %	Avg. ρ (CEA/NRG) / g/cm^3	Avg. closed porosity (CEA/NRG) / %	Grain size (CEA) / µm	Avg. crush load (CEA) / N	dpa (in Li_2TiO_3)
HT	0.06	LC	HT–0.06–LC	A	0.75	0.8–1.2	3.261	4.4	3.26	4.5	1–3	34	10.7
HT	7.5	LC	HT–7.5–LC	B	0.82	0.8–1.2	3.267	5.3	3.25	4.8	1.5–5	31	10.3
HT	11	LC	HT–11–LC	C	0.75	0.8–1.2	3.274	5.1	3.26	4.6	1.5–4	41	11.7
HT	11	HC	HT–11–HC	C	1.92	0.8–1.2	3.274	5.1	3.26	4.6	1.5–4	41	10.9
HT	30	LC	HT–30–LC	D	0.77	0.8–1.2	3.074	5.9	3.14	7.9	1–3	51	15.2
LT	7.5	LC	LT–7.5–LC_a	B	0.83	0.8–1.2	3.267	5.3	3.25	4.8	1.5–5	31	10.1
LT	7.5	LC	LT–7.5–LC_b	E	0.89	0.6–0.8	3.267	4.9	3.26	4.6	1–4	31	6.2
LT	7.5	HC	LT–7.5–HC	F	2.44	0.6–0.8	3.280	5.3	3.26	4.6	1–3	37	6.1
LT	11	HC	LT–11–HC	C	2.10	0.8–1.2	3.274	5.1	3.26	4.6	1.5–4	41	6.1
LT	30	LC	LT–30–LC	D	0.78	0.8–1.2	3.074	5.9	3.14	7.9	1–3	51	11.2

(see Fig. 1). The extent of the colour changes differs significantly. Most obvious is a grey and/or a bluish grey colour on the surface of the initially pale pebbles.

This is a common effect in a reducing atmosphere containing hydrogen where the oxygen content in Li_2TiO_3 decreases due to water formation as described in Eq. (1). The oxygen deficiencies are accompanied by a reduction of Ti(IV) in Li_2TiO_3 to Ti(III) leading to the change in colour.

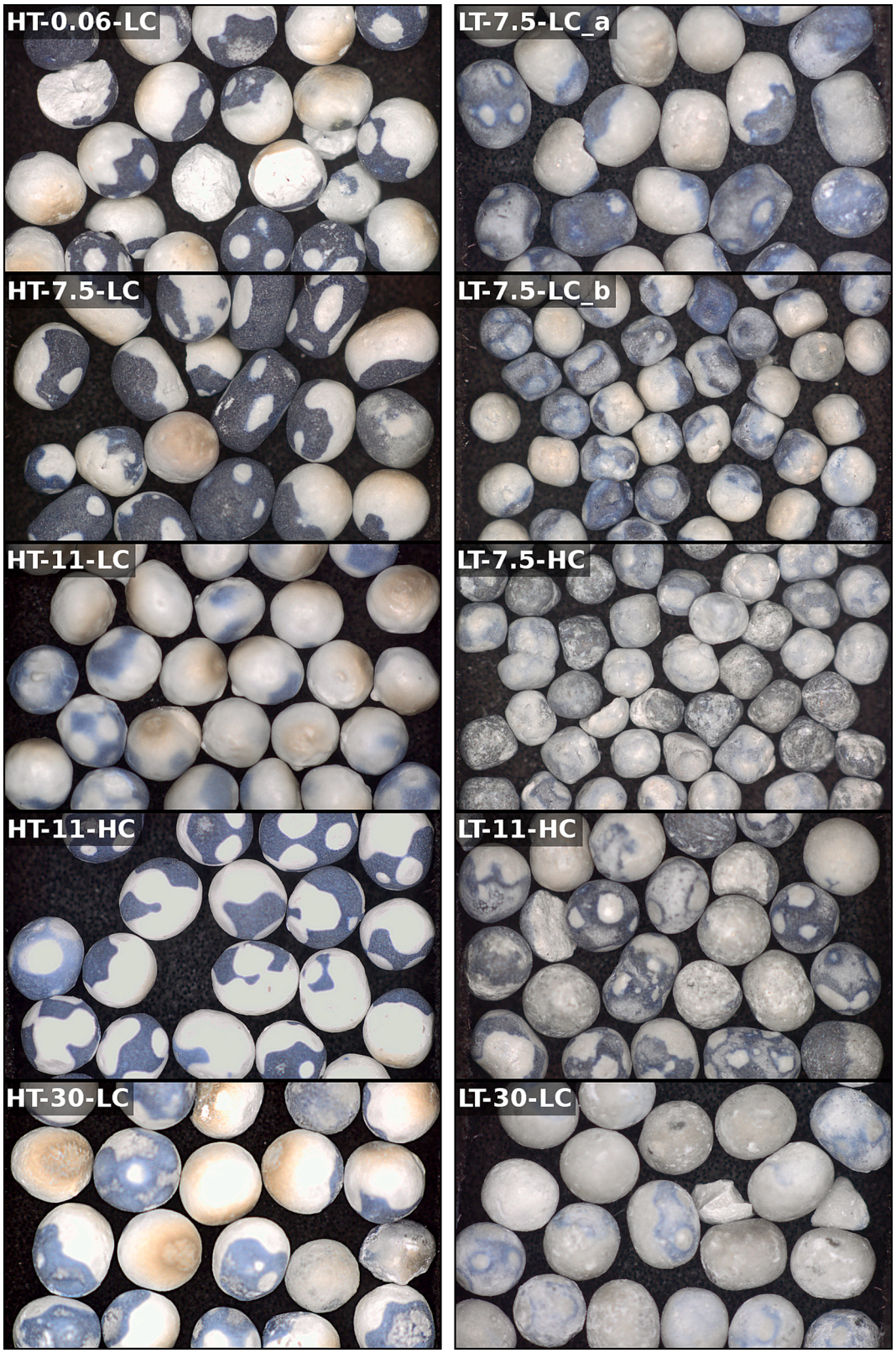

Fig. 1. Photos of some random pebbles irradiated at high (left) and at low temperatures (right). In each row, the lowest Li–6 content is at the top and the highest Li–6 content at the bottom.

$$x\ H_2 + Li_2TiO_3 \rightarrow Li_2TiO_{3-x} + x\ H_2O \quad (1)$$

Within the HICU experiment a gas mixture of neon and helium was used for temperature control. In the second containment, the helium gas contained 0.1 vol% of hydrogen. Therefore, the samples were irradiated in a slightly reducing atmosphere. In addition, oxygen defects in the ceramic pebbles were generated due to the irradiation with neutrons. Radiation-induced oxygen defects in Li_2TiO_3 were observed and described for example by Oyaidzu et al. and Suzuki et al. [9,10].

The change in oxidation state of Ti in darkened Li_2TiO_3 samples was proven for example by Wang et al. using X–ray photoemission spectroscopy (XPS) [11]. Oxygen defects were confirmed with the observation of E'-centres via electron spin resonance spectrometry (ESR) [12–14]. E'-centres are oxygen vacancies occupied by a single remaining electron [15]. In general, the dark colour vanishes by annealing the samples in air due to a recovery of the oxygen defects [14,16]. This was also observed within this study after an annealing of the samples during the TPD measurements.

Therefore, the oxygen defects and the consequential reduction of Ti (IV) to Ti(III) that lead to the change in colour is probably resulting from both the neutron irradiation and the slightly reducing atmosphere.

As previously mentioned, the degree of the colour change varies significantly and moreover, the dark colour is not homogenously distributed on the pebbles' surfaces (see Fig. 1). The pebbles remained white in parts. Sometimes big parts are still white with wavy borders to the dark parts, but there are also small round dots within the dark parts that remained white. The white dots bring up the assumption that the pebbles were touching and hence protecting each other in these spots. But this would imply that the larger white areas were also protected from an environment leading to a reduction of the Ti(IV), which cannot be proven. Furthermore, some pebbles show a high contrast between the white and the grey colour, other pebbles exhibit diffuse transition in colour. There seems to be a tendency that pebbles that were irradiated at high temperature show a higher colour contrast (cf., Fig. 1, left column). Moreover, if the colour contrast is relatively high for samples irradiated at low temperature (e. g. LT–7.5–LC_a, LT–11–HC), there is a transition of grey to bluish grey from the inner dark parts to the white parts, whereas in pebbles irradiated at high temperature, the darkened parts are homogenous in bluish grey colour.

Beside the grey and bluish grey colour change during the irradiation, some samples reveal a brown colour that is only observed in the white parts. Its extent is diffuse and it appears to exist only in the outermost surface of the pebbles, as it cannot be observed in the bulk of the few cracked pebbles. It makes the pebble surface look partly "burned". These brown parts are often ring shaped and sometimes the surface is slightly spalled in the middle of such a ring. This leads to the assumption that the pebble was sticking to the sample holder and the surface was damaged during the retrieval.

Such a colour change to brown was only described by Nakashima et al. when Li_2TiO_3 pebbles were purged with water instead of hydrogen [17]. As water is generated during the reduction reaction shown in equation 1 and also semi-tritiated water is formed, the pebbles were also exposed to a small amount of H_2O.

All but one of the samples (HT–11-HC) that were irradiated at high temperature clearly show this brown surface discolouration, whereas it can hardly be observed in samples irradiated at low temperature. Therefore, the high temperature during the irradiation most likely enhanced the brown discolouration. This would underline the assumption of a kind of "burning" of the pebbles in contact with the crucible wall lined with platinum.

For eight samples, an initial diameter range from 0.8 to 1.2 mm was given, whereas two samples had an initial diameter range of 0.6 to 0.8 mm (see Table 1). This fits mainly to the analyses made within the HICU PIE. The overall majority of the samples have pebbles lying within this range (see Table 2). However, most samples extend this range at the upper end. Although swelling could be a result of the irradiation, it would not be reasonable to that extent. Therefore, a discrepancy in the provided values of the unirradiated pebbles and the ones of PIE is more likely.

Table 2
Range in diameter for the majority (≥90 %) of the pebbles and the sphericity for all measured pebbles of each sample.

HT-samples	Ø range / mm	Sphericity	LT-samples	Ø range / mm	Sphericity
HT–0.06–LC	1.0–1.3 (~95 %)	0.77	**LT–7.5–LC_a**	1.0–1.3 (~91 %)	0.66
HT–7.5–LC	1.1–1.4 (~90 %)	0.66	**LT–7.5-LC_b**	0.7–0.9 (~92 %)	0.76
HT–11–LC	1.0–1.2 (~97 %)	0.84	**LT–7.5–HC**	0.7–0.9 (~91 %)	0.76
HT–11–HC	1.1–1.4 (~97 %)	0.80	**LT–11–HC**	1.0–1.3 (~97 %)	0.81
HT–30–LC	1.1–1.4 (~95 %)	0.82	**LT–30–LC**	1.0–1.3 (~95 %)	0.77

Fig. 1 further reveals the quite large variety of shapes among the pebbles. Whereas some samples (HT–0.06–LC, HT–11–LC, HT–11–HC, and HT–30–LC) appear to be relatively round, other samples show pebbles that vary from round to "egg-shaped" to almost cylindrical (HT–7.5–LC and LT–7.5–LC_a) or seem to be slightly square-cut (LT–7.5–LC_b and LT–7.5–HC). Table 2 includes the sphericity of each sample, which varies from 0.66 to 0.84. For pebbles appearing relatively round, sphericities with values close to 0.8 were measured. The samples that show almost a cylindrical shape exhibit as expected the lowest sphericity values of 0.66. These two samples with natural Li–6 abundance result from the same batch. The measured sphericity values do not always correspond directly to the appearance of the pebbles in Fig. 1, as these are just an exemplary sub-sample of the overall sample. Also, samples with a Li–6 content of 11 at% belong to the same batch. Here, the sample irradiated under a low constraint (HT–11–LC) exhibits a slightly higher sphericity than the samples irradiated under a high constraint (HT–11–HC and LT–11–HC). The other LC-HC couple (LT–7.5–LC_b and LT-7.5–HC) does not show this trend, but the samples result from two different batches.

3.2. Phase analysis

The phase content of the pebbles after the irradiation was investigated using XRD. Fig. 2 exemplarily shows the diffraction pattern of sample HT–11–LC. As expected, monoclinic Li_2TiO_3 is the main phase. Beside Li_2TiO_3, reflections of $Li_4Ti_5O_{12}$ can be observed. In comparison, a pristine sample – not from the same batch, but also provided by CEA – is displayed, which only shows the reflections of Li_2TiO_3. In contrast to Li_2TiO_3, $Li_4Ti_5O_{12}$ is depleted in lithium. $Li_4Ti_5O_{12}$ was formed during the irradiation due to the lithium transmutation and the associated lithium loss in the system. The formation of $Li_4Ti_5O_{12}$ due to a lithium burn-up can be derived from the TiO_2–Li_2O phase diagram [18], but – to the best of the authors' knowledge – it was not confirmed using phase analysis so far. Titanium in $Li_4Ti_5O_{12}$ has the same oxidation state of IV as in Li_2TiO_3.

Kleykamp observed a partial formation of cubic $LiTiO_2$ containing only Ti(III) under a reducing atmosphere at 900 °C [18]. The formation of such a phase must involve a loss in lithium, which fits to Kleykamp's non-stoichiometric composition of $Li_{1.92}Ti_{1.02}O_3$ [18]. Also, Hoshino et al. observed the formation of $LiTiO_2$ in non-stoichiometric $Li_{2-x}TiO_{3-y}$ samples with $Li_2O/TiO_2 = 0.9$ and 0.8, after annealing in a reducing atmosphere besides Li_2TiO_3 and $Li_4Ti_5O_{12}$. For stoichiometric Li_2TiO_3 or slightly non-stoichiometric $Li_{2-x}TiO_{3-y}$ ($Li_2O/TiO_2 \geq 0.95$) no phase with pure Ti(III) such as $LiTiO_2$ is observed [16] and the reduction of Ti (IV) is simply described as a result of a decreased oxygen content within the lithium metatitanate phase occurring in a reducing atmosphere as well as in vacuum [11,13,16,17,19,20]. Besides oxygen deficiencies and

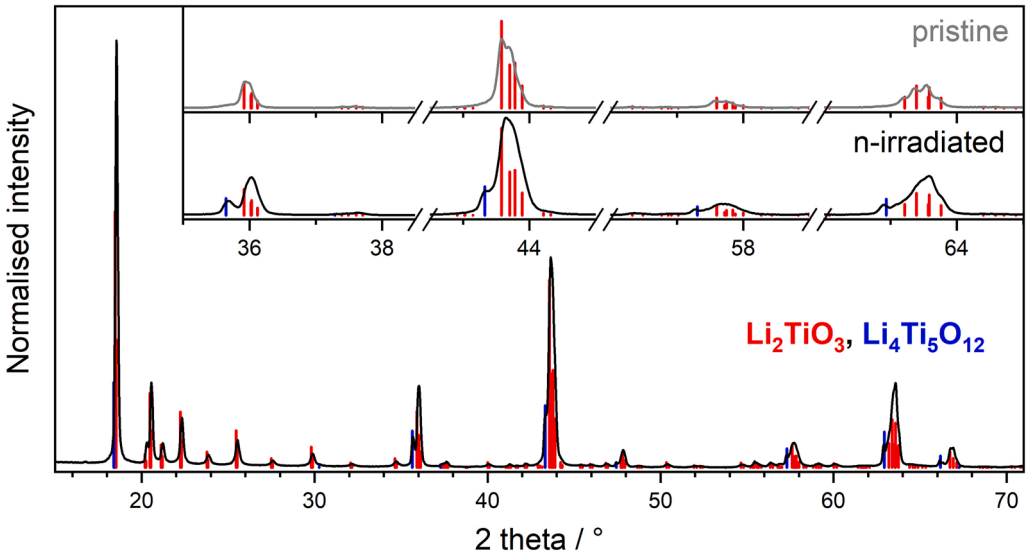

Fig. 2. XRD pattern of HT–11–LC (black) and reference positions of Li_2TiO_3 (red; [5]) and $Li_4Ti_5O_{12}$ (blue; [8]). In comparison, a pristine sample produced by CEA is shown. (For interpretation of the references to colour in this figure legend, the reader is referred to the web version of this article.)

a reduction of Ti(IV) to Ti(III), also the lithium content was reduced due to the lithium transmutation during the HICU neutron irradiation. Hence, also the partial formation of $LiTiO_2$ could have occurred in the HICU samples if the Li_2O/TiO_2 ratio in the samples was reduced below 0.95.

The reflection positions of $LiTiO_2$ (e.g. COD# 1541630, i.e. [21]) fit in the recorded diffraction pattern, but they would be superimposed completely by the reflections of Li_2TiO_3. The reflection peaks are too broad to resolve the possibly occurring reflections from both phases as it could be shown by Hoshino et al. [16]. Therefore, the existence of $LiTiO_2$ cannot be completely excluded. However, it is more likely that the reduced titanium Ti(III) is included in the crystal structure of lithium metatitanate in the form of $Li_{2-x}TiO_{3-y}$ as described by Hoshino et al. [19]. This is supported by a shift of the reflection positions after the annealing of a sample in synthetic air and the accompanied oxidation of the titanium (see Fig. 3). Ti(III) is larger than Ti(IV) and hence, the expanded cell, including Ti(III), is reduced again during oxidation and a slight shift to higher 2 theta values is observed (the effective ionic radii in sixfold coordination are: Ti(III) = 0.670 Å and Ti(IV) = 0.605 Å [22]).

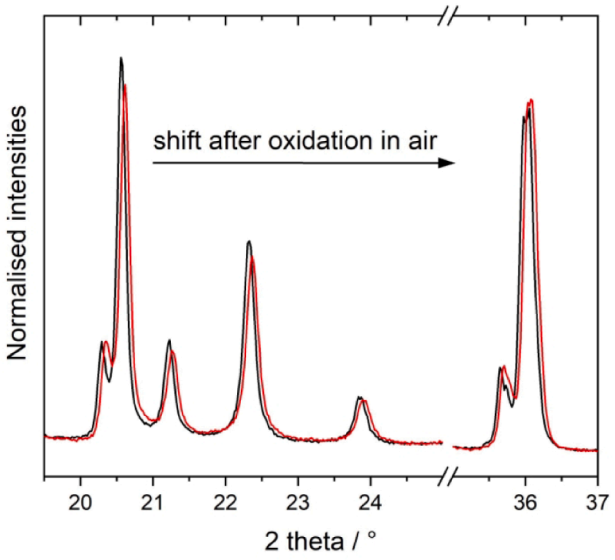

Fig. 3. After the oxidation in synthetic air, a slight shift to higher 2 theta values is observed in XRD patterns (here: HT–11–HC before (black) and after oxidation (red)). (For interpretation of the references to colour in this figure legend, the reader is referred to the web version of this article.)

Rietveld refinements were performed for all diffraction patterns including the crystal structures of monoclinic Li_2TiO_3 [5] and cubic $Li_4Ti_5O_{12}$ [8]. The resulting weight percentages of each phase are plotted versus the initial Li–6 content in Fig. 4. There is a tendency that the amount of Li_2TiO_3 decreases, while the amount of $Li_4Ti_5O_{12}$ increases with increasing initial Li–6 content. However, especially the samples irradiated at high temperatures with an initial Li–6 content of 11 at% rarely follow the trend. Samples that were pre-compressed (i.e. high constraint) were not included in the fit of the trendline. With regard to the irradiation temperature, no clear trend was observed.

3.3. Microstructure

A direct comparison of the pebbles before and after the irradiation is not possible as no microscopic images of the pristine samples are available.

Cross sections of the irradiated pebble samples in the optical microscope reveal comparable shapes as within the visual and geometrical inspection. Fig. 5 exemplarily shows an optical micrograph of a sample irradiated at high temperature and one irradiated at low temperature, both with natural lithium abundance.

Within the bulk, all pebbles exhibit relatively big cracks and cavities. Cavities are typically formed during the applied fabrication method (extrusion-spheronisation) of the Li_2TiO_3 pebbles [4,23]. Some samples (e. g., HT–0.06–LC, LT–11–HC, LT–30–LC) also show relatively big pores. Often the pores are ragged in shape. Furthermore, all samples show many fine round pores distributed within the pebble. The fine pores are often elongated and ragged and partly agglomerate. Sample HT–11–LC is an exception, as it appears relatively dense with fine pores besides big cavities in the centre of almost each pebble. There is no trend for the observed pores, cracks and cavities and the irradiation temperature, the Li–6 content, nor the constraint of the pebble bed.

Almost all samples exhibit a light grey layer in their border region (see Figs. 5 and 6). This layer often occurs only in parts of the border region and varies in its thickness. This fits well to the partial colour change observed on the surface of the pebbles within the visual inspection. A clear trend is observed for these layers with regard to the irradiation temperature. Pebbles irradiated at low temperature show layer thicknesses of about 10–20 μm. This is also true for samples that

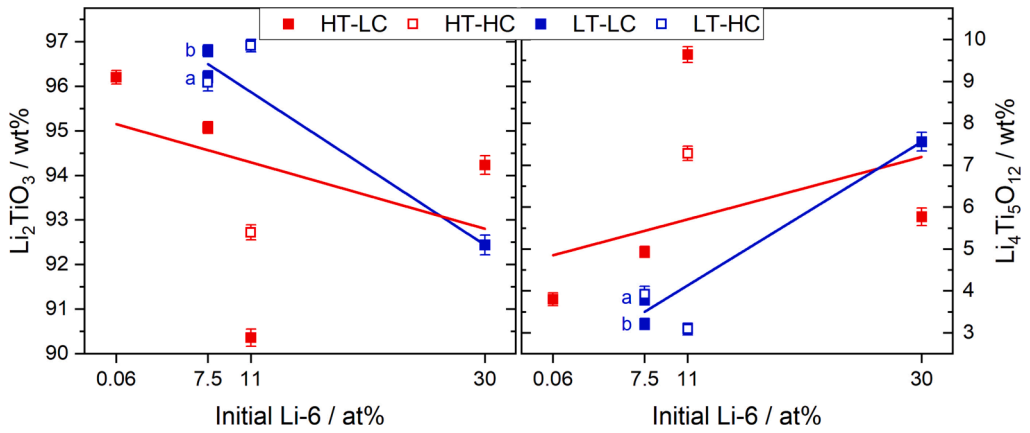

Fig. 4. Amounts of Li_2TiO_3 and $Li_4Ti_5O_{12}$ in the different samples determined from Rietveld refinements versus their initial Li–6 content. Open symbols (high constraint samples) were not included in the fitting of the trend line.

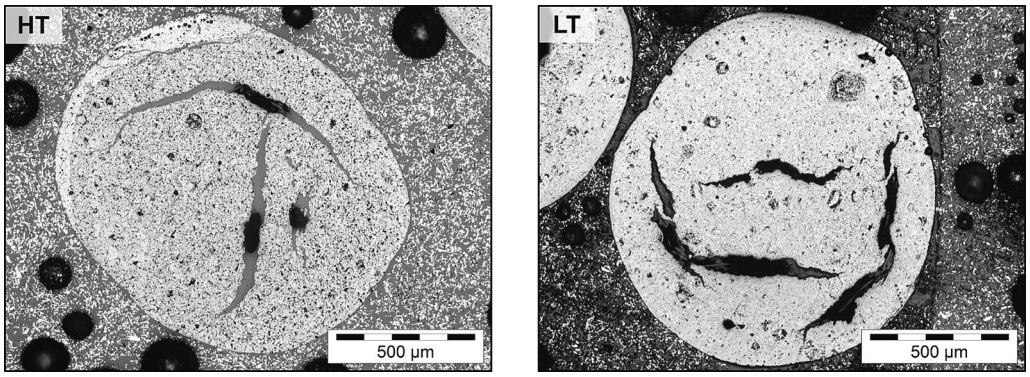

Fig. 5. Optical micrographs of cross sections of a sample irradiated at high (left; HT–7.5–LC) and a sample irradiated at low temperature (right; LT–7.5–LC_a).

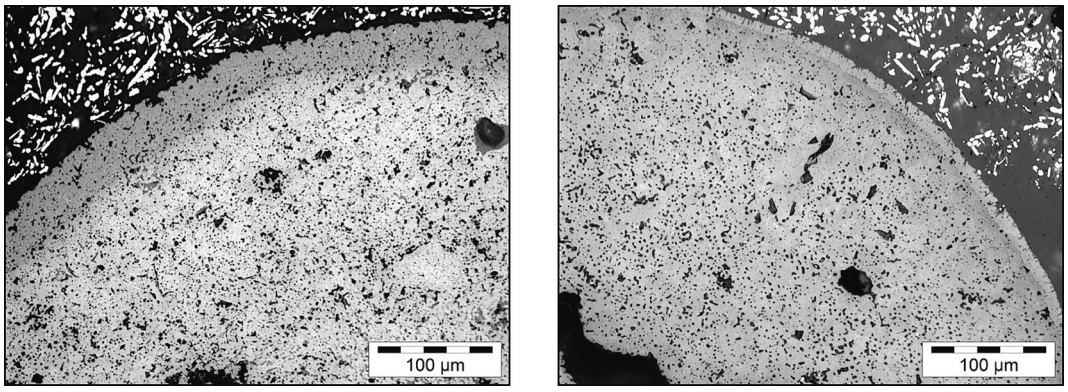

Fig. 6. Selected optical micrographs of a sample irradiated at high temperature showing a relatively thick grey layer in the border region (left: HT–7.5–LC) and of a sample irradiated at low temperature with a significantly thinner layer (right: LT–7.5–LC_b).

show a relatively intense colour change on the surface such as LT–7.5–LC_a or LT–11–HC (compare Fig. 1). In comparison, the layers in pebbles irradiated at high temperature are significantly thicker (see Fig. 6). Pebbles irradiated at high temperature often exhibit layer thicknesses of about 50 µm and in some cases even up to ~80 µm. There appears to be no relation between the layer thickness and the Li–6 content of the samples. In sample HT–11–LC, a light grey layer was detected within a cavity in the centre of one pebble.

The microstructure on the surface and within the bulk of the irradiated HICU pebbles was investigated using SEM. While the surface of some pebbles is relatively smooth (see Fig. 7, left), other pebbles exhibit defects such as cracks and open cavities (see Fig. 7, right). The microstructure of the pebbles' surfaces varies from relatively dense to expanded grain to porous boundaries. The different types of microstructure are not specific for certain samples or batches. The microstructure of the surface not only varies between different samples, but also within one sample. There seems to be no correlation of the observed microstructure and the Li–6 content nor the irradiation conditions such as the temperature or the constraint of the pebble bed.

Several samples show more or less significant "bulges" (see Fig. 8). It should be noted here that these "bulges" do not stick out in reality, but only appear as a 3D structure in the SEM images. Often only roundish

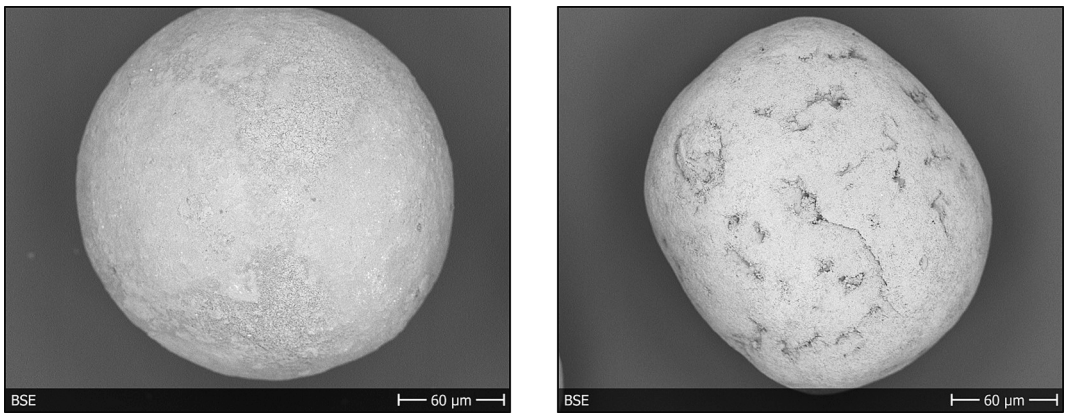

Fig. 7. Examples for pebbles showing a significantly smooth surface (left; LT–30–LC) and surface with relatively many defects (right; LT–7.5–LC_a). (Backscattered electron (BSE) image mode.).

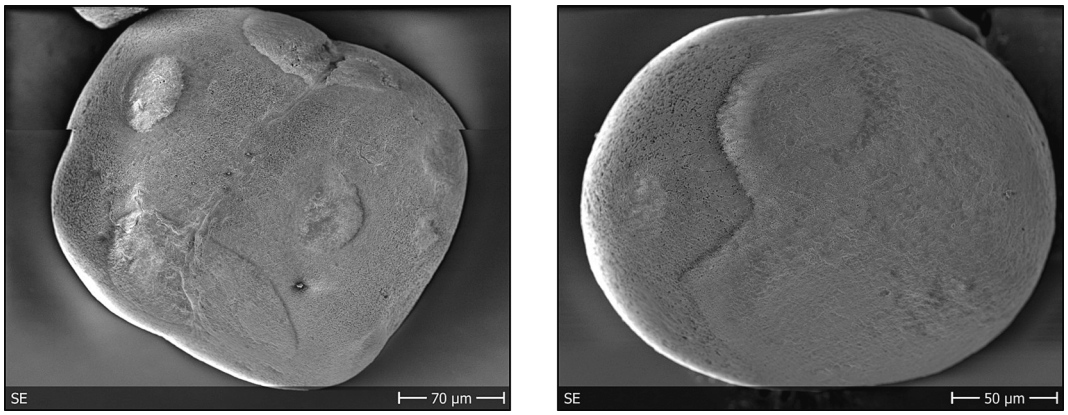

Fig. 8. Examples (left: HT–7.5–LC, right: HT–11–HC) for pebbles showing "bulges" on their surfaces, frequently with wavy borders. (Secondary electron (SE) image mode.).

"bulges" can be observed, but sometimes the wavy shapes of the "bulges" fit to those of the dark/pale boundaries observed within the visual inspection (compare Fig. 1). Due to the curved surface it is hard to derive information from the material contrast, which is relatively low in the images from backscattered electrons (BSE). In all cases, the microstructure of the "bulges" seems denser compared to the rest of the surfaces showing often slightly expanded grain boundaries. A correlation in observing these "bulges" on the surface and the irradiation temperature cannot be observed. However, only a relatively small amount of the pebbles' surfaces was investigated with SEM compared to the visual inspection and only one side is visible in the SEM.

Cross sections of the different HICU pebble samples investigated with SEM reveal a similar impression given by the cross sections used in the optical microscope. Fig. 9 exemplarily shows micrographs of one sample irradiated at high temperature and of one irradiated at low temperature, both with natural lithium abundance.

Most samples reveal a microstructure including many fine pores. Sometimes these pores are agglomerated to pore voids. Often the samples exhibit relatively large cracks that especially occur in the centre of the pebbles. Large cracks can hardly be observed in the border regions. Some pebbles also reveal cavities in the bulk. This is characteristic for the fabrication process [4,23]. As mentioned previously for the surface, the microstructure in the bulk varies from relatively dense to quite porous. Fig. 10 demonstrates different examples for the differences in the appearance of pores. Although some samples appear to be slightly more porous (e. g., HT–0.06–LC, HT–30–LC, LT–11–HC, or LT–30–LC) and others seem to have a denser microstructure if big cracks and cavities are not considered (e. g., HT–11–LC, LT–7.5–LC_a or LT–7.5–HC), the microstructure can vary within one sample. Again, all pebbles in sample HT–11-LC exhibit a dense microstructure with fine pores and almost all pebbles have big cavities in the centre. There seems to be no clear relation of the size and the number of pores and the irradiation temperature, the Li–6 content or the constraint applied to the pebble bed. In some samples, it is possible to distinguish the different grains. The grain size varies from about 5 to 10 µm and rarely it is about 20 µm. As the grain size ranged from about 1–5 µm in the pristine samples (cf., Table 1), a moderate grain growth took place during the irradiation at elevated temperatures. In some cases, grains grew to a stronger extent. However, there is no apparent correlation between the degree of the grain growth and the irradiation temperature.

The formation of a 'crust' on the surface of neutron-irradiated Li_2TiO_3 pebbles was also observed by van Til et al. [23]. However, the reduced oxygen content was only explained by the used reducing gas atmosphere.

Also, in the SEM images (see Fig. 9 and Fig. A1 in the supplementary information), the occurrence of the light grey layer in the border regions is conspicuous. Underlining the results from the optical microscopy, the layers of samples irradiated at high temperature are relatively thick, while the layers in pebbles irradiated at lower temperature are much thinner (see Fig. 9). In some samples, the secondary phase can also be observed within the bulk (see light grey small and often elongated shapes in Fig. 10, top). Besides the examples shown, the second phase is also sometimes concentrated near pores or at grain boundaries.

EDS analyses on selected samples show a higher Ti/O ratio in the light grey layers compared to the adjacent darker bulk regions. As the measurements for oxygen is commonly error-prone, no direct values can

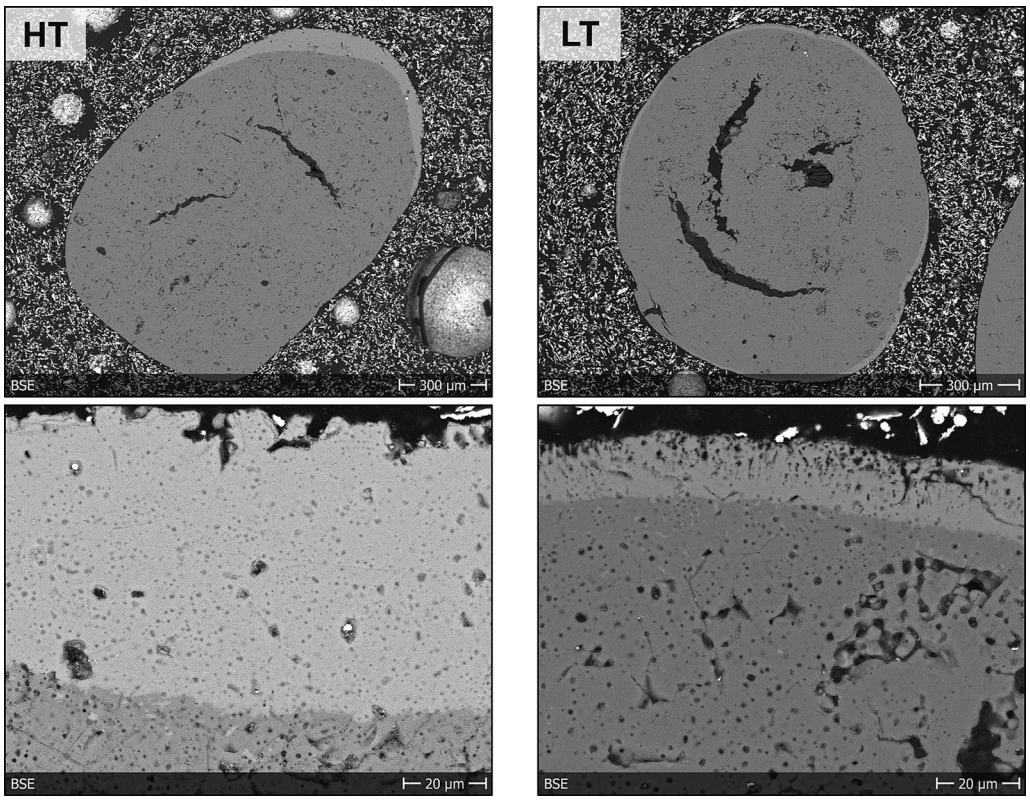

Fig. 9. Cross sections of samples with natural lithium abundance irradiated at high temperature (left; HT–7.5–LC) and at low temperature (right; LT–7.5–LC_a). The BSE image mode reveals a layer in the border region that is in general much thicker for samples irradiated at high temperature.

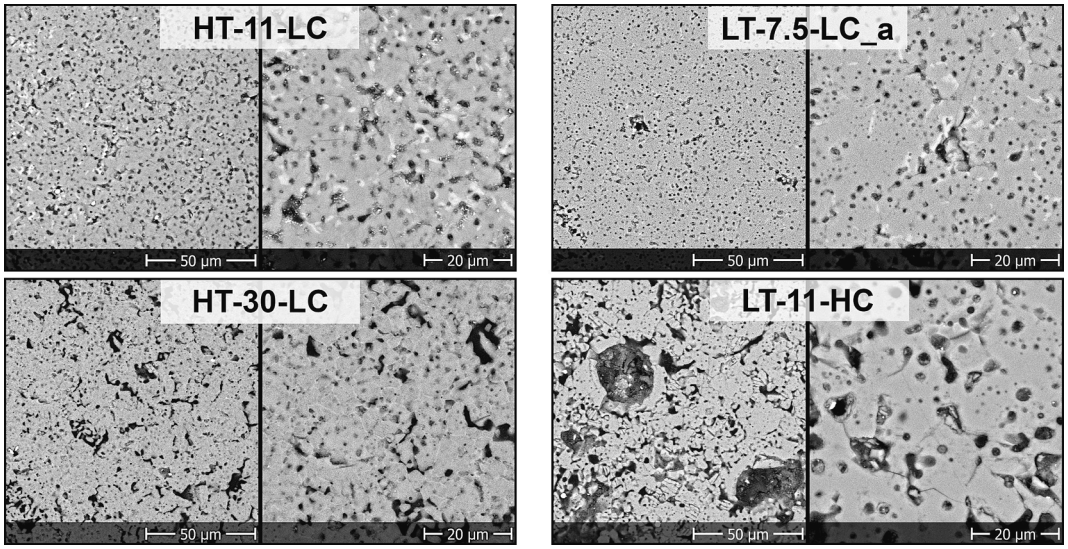

Fig. 10. BSE micrographs of selected samples irradiated at high (left) and at low temperatures (right) with a relatively dense structure (top) or with more and bigger pores (bottom). Moreover, a second phase in lighter grey can be observed within the bulk in the samples shown at the top.

be derived. However, $Li_4Ti_5O_{12}$ has a higher Ti/O ratio in comparison to Li_2TiO_3. Therefore, it can be assumed that the light grey phase is $Li_4Ti_5O_{12}$.

The lithium transmutation should take place relatively homogeneously within the pebble. This would fit to the occasionally observed finely dispersed second phase within the bulk. However, oxygen defects are probably more likely generated on the pebble's surface and thus the formation of the secondary phase is enhanced.

Furthermore, the layers could be related to an evaporation of lithium. A significant evaporation of lithium is not expected as in comparable Li_2TiO_3 pebbles no lithium loss was observed at even higher temperatures of 970 °C in long-term annealing experiments after 96 days [24]. Nevertheless, in other studies such as Otani et al. a lithium loss in lithium metatitanate pebbles were observed after the annealing at 900 °C for 1000 h in a helium atmosphere with additions of 1 % hydrogen [25]. However, the effect of lithium evaporation is larger in hyperstoichiometric lithium metatitanates [25,26]. Although the pebbles in the present study consisted of stoichiometric Li_2TiO_3 in the

pristine state, an evaporation of lithium affecting the formed layers at the surface cannot be exluded.

3.4. Density and porosimetry

The densities of the irradiated pebbles measured by helium pycnometry have an average value of 2.7 ± 0.1 g/cm^3. Therefore, the densities decreased on average by 0.5 ± 0.1 g/cm^3 or by 17 ± 4 % after the irradiation. With 0.8 g/cm^3 sample HT–11–LC has the most significant decrease in comparison to the pristine sample. The measured density values and their standard deviations (*SD*) for all samples are listed in Table 3. Moreover, the decrease in density with regard to the pristine samples are summarised in Table 3.

Based on the *TD*, the closed porosity can be derived from the density values. The closed porosity was calculated using a *TD* = 3.415 g/cm^3 for Li_2TiO_3 [5]. It was assumed that the irradiated pebble samples only consist of pure Li_2TiO_3. The average closed porosity is 21 ± 4 %. Hence, the closed porosity of the pebbles increased from about 6 ± 2 % (for the pristine samples) on average by 16 ± 4 percentage points (pp) during the irradiation. The aforementioned sample HT–11–LC has a deviation of + 23 pp with regard to the closed porosity. The closed porosity for each sample and its increase compared to the pristine samples is given in Table 3 and displayed in Fig. 11. The increase of the closed porosity probably results from a combination of the lithium loss and the decrease of the open porosity during "sintering" at elevated temperatures. However, there is no data for the latter available, which is why this cannot be confirmed. No correlation of the closed porosity or its increase during irradiation can be observed with regard to the irradiation temperature nor the initial batch/Li–6 content.

From the XRD analyses, it is known that at least $Li_4Ti_5O_{12}$ is present in the irradiated samples, which has a *TD* of 3.49 g/cm^3 [8]. The questionable third phase $LiTiO_2$ has an even higher *TD* of 4.06 g/cm^3 [21]. To estimate a possible error for the resulting closed porosities, two assumptions were made: the pebbles were assumed to be perfect spheres with a diameter of 1 mm and have a spherical shell with a thickness of 50 μm. The bulk and half of the spherical shell is assumed to be Li_2TiO_3, while the other half of the shell differs from Li_2TiO_3.

In the case, that half of the spherical shell is $Li_4Ti_5O_{12}$, the *TD* would be 3.43 g/cm^3 and the difference in the derived closed porosity would be negligible. For the "worst case scenario" it was assumed that half of the spherical shell consists of $Li_4Ti_5O_{12}$:$LiTiO_2$ in the ratio 1:1, which would result in a *TD* of 3.46 g/cm^3. In this latter case, the closed porosity values given here calculated with the *TD* of pure Li_2TiO_3 would be underestimated by about 1 pp.

Furthermore, there is no apparent correlation between the observations in optical and SE micrographs and the density or closed porosity values. For some samples, the microscopic observations fit to the data, for some they do not. Samples HT–0.06–LC and HT–30–LC exhibit many pores and cracks in the cross sections and they also have a relatively low density/high closed porosity. However, while sample LT–11–HC reveals many pores in the micrographs, it shows the highest density and the lowest closed porosity values. Beside some cavities, the bulk of sample HT–11–LC seems to be relatively dense, it has the lowest density and hence, the highest closed porosity.

3.5. Mechanical characterisation

To evaluate the mechanical strength of the irradiated Li_2TiO_3 pebbles, crush load tests were performed. The variation of the crush load values is relatively high and the average values of all samples range from 19 to 40 N. Also, the standard deviations within a sample are relatively high. The sphericity for example is expected to affect the variation of the average crush loads, as well as the standard deviations. Table 4 lists all average crush load values and their standard deviations. In addition, the decrease with regard to the pristine samples is given. Again, there is a strong variation in how much the crush load decreased from the initial value. The range of decrease in crush loads is relatively large and reaches from 3 to 44 % (see Table 4). Considering the standard deviation, the decrease for the samples HT–11–LC and HT–11–HC is insignificant. Fig. 12 demonstrates the crush load values of the samples (blue) and the absolute value of their decrease after the irradiation (red). It needs mentioning that crush load values strongly depend on the size of the pebble used and on the device. As there is no information about the parameters used for the analysis of the unirradiated pebbles, a direct comparison is difficult. What can be said, is that there is no apparent correlation of the crush load values themselves or the deviation from the initial values regarding the irradiation temperature, the initial Li–6 content, nor the dpa value that was calculated for each sample. A plot displaying the crush load versus the dpa level is shown in Figure A2 in the supplementary information. Although there is no trend, it can be concluded that the reduction in crush load is not larger for samples that experienced higher dpa levels. The only samples that show a similar behaviour in Fig. 12 are the two samples HT–7.5–LC and LT–7.5–LC_a. They exhibit similar average crush loads after the irradiation and as they originate from the same batch and had the same initial crush load value, they also show a similar decrease. For the sample couple HT–11–HC and LT–11–HC originating from the same batch, this is not the case. The crush load values are not related to the closed porosity values of the samples. Moreover, the absolute deviations of these values to the pristine samples show no correlation (cf., the decrease in crush loads and the increase in closed porosity in Figs. 12 and 11, respectively).

As for samples LT–7.5–LC_b and LT–7.5–HC pebbles with smaller diameters had to be used for the uniaxial crush load tests, it was expected to observe relatively low crush load values. This might be true for LT–7.5–LC_b with 23 N, but not for LT–7.5–HC with 31 N. The quite low sphericity and the partly occurring cavities and large cracks have a high influence on the uniaxial crush load tests, which leads to high variations and no clear trends.

However and as expected, the average crush loads decreased after the irradiation in all cases. On the one hand, the pebbles experienced radiation-induced damages and chemical changes. On the other hand, the pebbles undergo a thermal anisotropic expansion during cooling after the irradiation from relatively high irradiation temperatures. The anisotropy is due to the non-cubic crystal structure of the occurring Li_2TiO_3. The expansion during cooling leads to microcracks and a deterioration of the mechanical strength of the pebbles within the PIE (cf., thermal cycling tests [27]). It is suggested that the mechanical stability is not degraded significantly if the samples are kept above a certain material specific temperature due to the continuous healing of

Table 3
Densities (ρ) determined from He pycnometry and closed porosities derived from density values and their decrease/increase compared to pristine samples. The *TD* of pure Li_2TiO_3 was used to calculate the closed porosity (see text for estimated deviations). An error of 1 % is estimated for the closed porosity. (*SD* = standard deviation, pp = percentage points.).

HT-samples	ρ / g/cm^3	*SD* / g/cm^3	Decrease / %	Closed porosity / %	Increase / pp	LT-samples	ρ / g/cm^3	*SD* / g/cm^3	Decrease / %	Closed porosity / %	Increase / pp
HT–0.06–LC	2.6	0.005	19	23	18	**LT–7.5–LC_a**	2.7	0.005	18	22	18
HT–7.5–LC	2.7	0.003	16	20	15	**LT–7.5–LC_b**	2.6	0.003	19	23	18
HT–11–LC	2.5	0.004	24	28	23	**LT–7.5–HC**	2.9	0.004	12	17	12
HT–11–HC	2.8	0.002	13	17	12	**LT–11–HC**	2.9	0.005	12	16	11
HT–30–LC	2.5	0.004	21	27	19	**LT–30–LC**	2.7	0.002	14	21	13

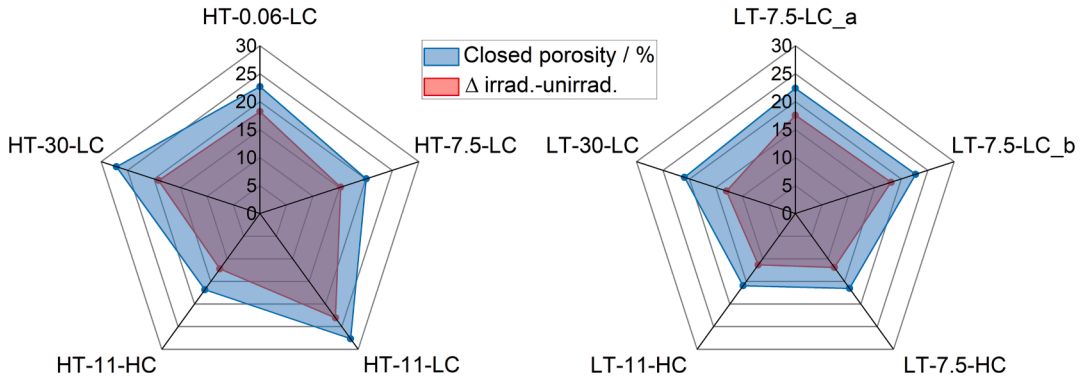

Fig. 11. Closed porosities (blue) and their increase compared to the pristine pebbles (red) for samples irradiated at high (left) and at low temperatures (right). (For interpretation of the references to colour in this figure legend, the reader is referred to the web version of this article.)

Table 4
Crush load values with standard deviations (SD) for all samples and their decrease compared to pristine samples. In addition, the diameter of the pebbles used in the crush load tests is given.

HT-samples	Crush load / N	*SD* / N	Decrease / %	Pebble Ø / mm	LT-samples	Crush load / N	*SD* / N	Decrease / %	Pebble Ø / mm
HT–0.06–LC	19	6	44	1	**LT–7.5–LC_a**	24	11	23	1
HT–7.5–LC	23	8	26	1	**LT–7.5–LC_b**	23	10	25	0.7
HT–11–LC	40	12	3	1	**LT–7.5-HC**	31	9	16	0.7
HT–11–HC	39	10	6	1	**LT–11–HC**	29	7	29	1
HT–30–LC	40	11	22	1	**LT–30–LC**	40	8	21	1

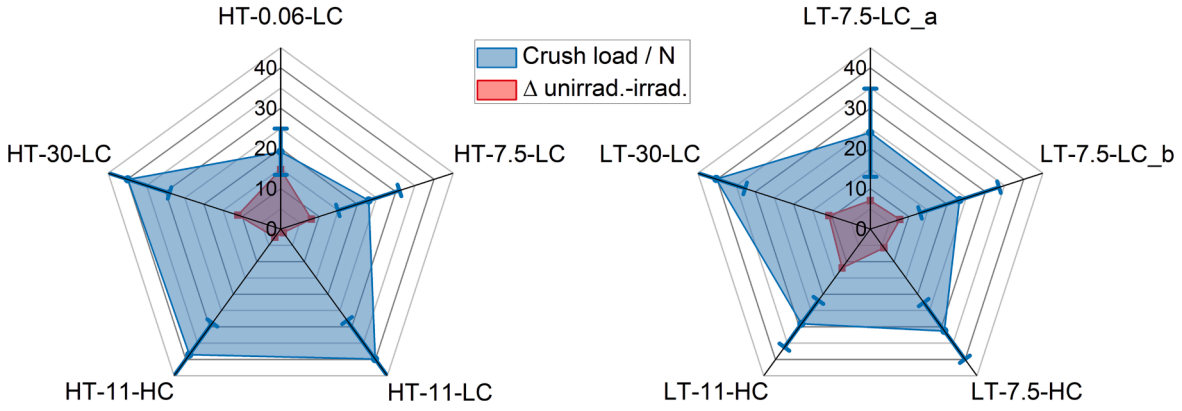

Fig. 12. Average crush loads of the irradiated pebbles (blue) and the absolute values of their deviation compared to pristine pebbles (red) plotted for samples irradiated at high (left) and at low temperatures (right). (For interpretation of the references to colour in this figure legend, the reader is referred to the web version of this article.)

microcracks [27].

3.6. Tritium release behaviour

The tritium release of the Li_2TiO_3 pebbles was analysed within the HICU PIE by recording the activity during a TPD experiment. The development of the specific release rates in dependence on the temperature for all samples irradiated at high and at low temperatures is shown in Fig. 13 left and right, respectively. In general, the samples irradiated at high temperature show significantly lower specific release rates in comparison to the samples irradiated at low temperature (consider the scaling of the y-axes in Fig. 13). Therefore, the tritium inventories for samples irradiated at a low temperature lie above those for samples irradiated at high temperature. Tritium was released more easily during the irradiation period taking place in a higher temperature range correlating to the peak temperature in the tritium release experiments. Therefore, this tritium was already released during the irradiation itself and was no longer available for the desorption measurements. The same trend is observed and described for lithium silicate samples of this irradiation campaign by Heuser et al. [3]. Actually, the average tritium inventory in LT–samples ($1.2 \cdot 10^8 \pm 7.7 \cdot 10^7$ Bq/g) is about 20 times higher than in HT–samples ($6.0 \cdot 10^6 \pm 1.8 \cdot 10^6$ Bq/g). The tritium inventory after heating as shown in Fig. 13 and the total tritium inventory including the heating period, the dwell time and the cooling period for each sample are given in Table 5.

For all samples, the tritium release starts very slowly at about 300 °C and increases more rapidly at temperatures above 450 °C. All samples show one main release peak in the region of 770 to 940 °C. The release peak temperatures are very similar on average for both irradiation temperatures (see Table 5). The tritium release curves vary for all samples from narrower to broader curve shapes. Moreover, there are asymmetries leading to tails on the left or on the right side of the main peak. In the case of the two high constraint samples HT–11–HC and LT–11–HC, there seems to be a higher asymmetry with a flatter decrease

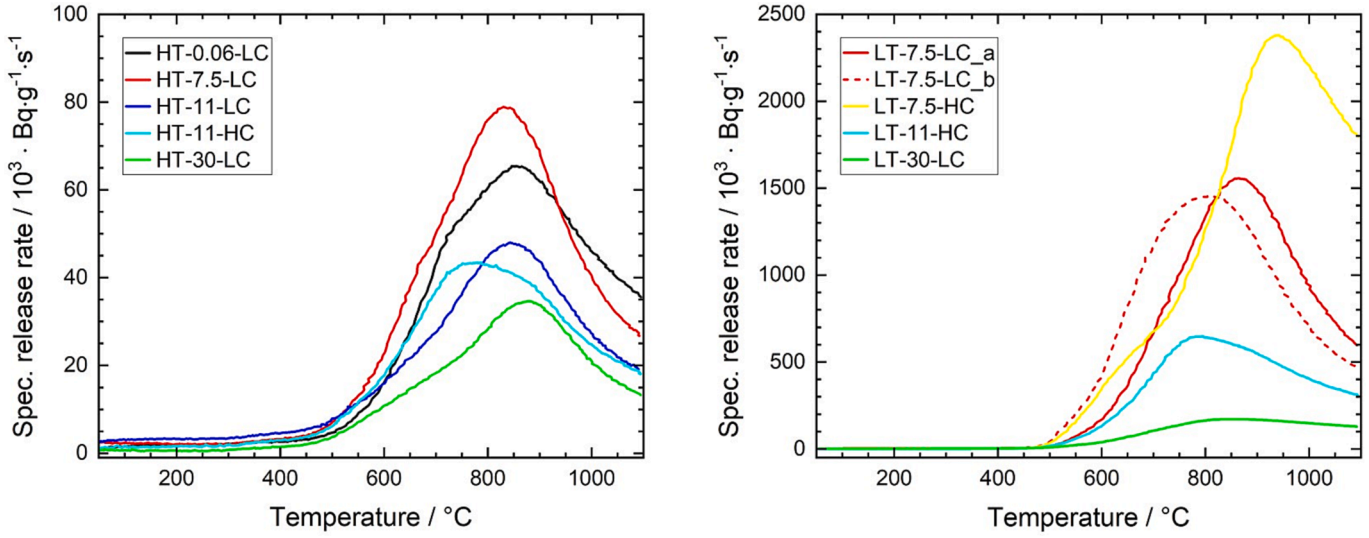

Fig. 13. Specific tritium release rates of pebble samples irradiated at high (left) and at low temperature (right).

Table 5
Peak temperatures in the specific release curves and tritium inventories (total for the whole measurement incl. heating, dwell time and cooling, and only after heating as plotted in Fig. 13).

HT-samples	T_{peak} / °C	Total T inv. / Bq/g	T inv. after heating / Bq/g	LT-samples	T_{peak} / °C	Total T inv. / Bq/g	T inv. after heating / Bq/g
HT–0.06–LC	859	$1.9 \cdot 10^7$	$7.4 \cdot 10^6$	**LT–7.5–LC_a**	865	$2.5 \cdot 10^8$	$1.4 \cdot 10^8$
HT–7.5–LC	839	$1.5 \cdot 10^7$	$8.3 \cdot 10^6$	**LT–7.5–LC_b**	804	$2.6 \cdot 10^8$	$1.5 \cdot 10^8$
HT–11–LC	847	$1.3 \cdot 10^7$	$5.5 \cdot 10^6$	**LT–7.5–HC**	942	$7.5 \cdot 10^8$	$2.2 \cdot 10^8$
HT–11–HC	772	$1.2 \cdot 10^7$	$5.3 \cdot 10^6$	**LT–11–HC**	796	$1.5 \cdot 10^8$	$6.8 \cdot 10^7$
HT–30–LC	876	$8.1 \cdot 10^6$	$3.7 \cdot 10^6$	**LT–30–LC**	858	$5.6 \cdot 10^7$	$2.0 \cdot 10^7$

after the maximum. However, this is not observed for the sample LT–7.5–HC. For each sample series, there is no clear trend for the extent of the specific release rate regarding the initial Li–6 content. However, the samples enriched with Li–6 above its natural abundance show relatively low release rates in their temperature regimes. And the two samples with 30 at% enrichment in Li–6 show even the lowest specific release rates with regard to the irradiation temperature. The opposite might have been expected, as in theory more lithium could have been transmuted with the higher Li–6 enrichment. For the lithium silicate samples included in the HICU experiment a difference between the irradiation temperatures was observed [3]. While the peak maxima of samples irradiated at about 650 °C is in a comparable range, the peak maxima of samples irradiated at 800–850 °C are shifted to lower release temperatures for lithium silicate samples [3].

Van Til et al. investigated the tritium release behaviour in comparable Li_2TiO_3 pebble samples (i.e. from the same producer) after the EXOTIC 9/1 irradiation experiment [28]. Samples with an initial natural lithium abundance show a tritium release at an average temperature of 700 °C, which is slightly lower than the release temperatures in the present study. In contrast to the present study, in [28] a more or less constant release between 200 and 600 °C and again at about 900 °C was observed for samples enriched with 30 at% Li–6. However, the used enriched samples by van Til et al. showed a lot of closed porosity that can act as trapping sites for the generated tritium. Within the HICU PIE no correlation between the tritium release behaviour and the closed porosity can be derived. Tritium release temperatures observed in thermal desorption measurements by Kinjyo et al. for Li_2TiO_3 provided by CEA are significantly lower [29]. Different purge gases based on nitrogen were used in their case. The most comparable purge gas composition, nitrogen with additions of hydrogen, shows an asymmetric tritium release peak around 400 °C. There can be several reasons for this deviation in the main desorption temperature. On the one hand, this could result from material properties such as a higher open porosity in the pebbles enhancing the tritium release. On the other hand, lower desorption temperature could result from much shorter neutron irradiation time of 100 min [29] in comparison to more than one year in the present study. Due to the shorter irradiation not as much tritium was generated deep within the bulk. Moreover, the time span between the neutron irradiation and the out-of-pile tritium release measurements was presumably much larger in the case of the HICU experiment. In the case that the time is short, also more loosely bonded tritium is released and hence, less energy is needed. In the present study the tritium release measurements were performed several years after the irradiation and hence, there is more tritium that is tightly bonded to the material. Irradiation temperatures observed by Yang et al. in Li_2TiO_3 pebbles are with around 660 °C only slightly lower [30]. Again, this can have different reasons. Beside a probable shorter time between the irradiation and the desorption measurements, also the different fabrication process can lead to differences in the material properties that can influence the tritium release behaviour. Although several studies exist on the tritium release behaviour, they are often not directly comparable and often detailed information about the material properties are missing.

QMS measurements were performed to obtain additional information about the gaseous species that were released during the TPD. The detectability of the selected masses (m) is given in Table 6 for each sample. Fig. 14 shows gaseous species of the selected masses released during the TPD. It should be noted that the values of partial pressure (p_p) can only be compared within one measurement. Therefore, no quantitative information among the different samples can be derived. Factors were used for the different QMS signals to implement them in one plot. Moreover, the original curves of masses m–6, m–19, m–20, and m–22 are very noisy and were smoothed for plotting using the Savitzky-Golay method with 20 points and the polynomial order of two.

As described in the experimental section, helium with additions of

Table 6
Detection of selected masses (m) of all samples during TPD. (● = detectable, ○ = signal slightly > background noise, / = not detectable.).

Sample	m–2 H_2	m–3 T, He-3	m–4 He–4, HT	m–6 T_2	m–18 H_2O	m–19 OT	m–20 HTO	m–22 T_2O
HT–0.06–LC	●	●	●	/	●	○	○	/
HT–7.5–LC	●	●	●	/	●	●	○	/
HT–11–LC	●	●	●	/	●	○	○	/
HT–11–HC	●	●	●	/	●	○●	○	/
HT–30–LC	●	●	●	/	●	○●	○	/
LT–7.5–LC_a	●	●	●	/	●	●	●	/
LT–7.5–LC_b	●	●	●	/	●	○	○	/
LT–7.5–HC	●	●	●	/	●	○	○	/
LT–11–HC	●	●	●	/	●	○	○	/
LT–30–LC	●	●	●	/	●	○	○	/

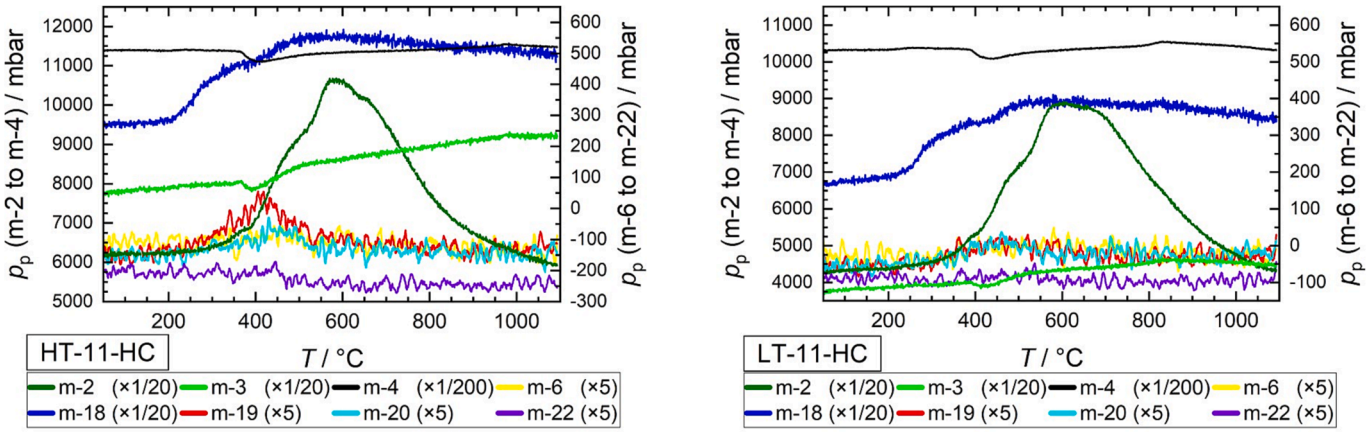

Fig. 14. Selected masses (m) for two exemplary samples irradiated at HT (left, HT–11–HC) and at LT (right, LT–11–HC). The partial pressures (p_p) of the QMS signals were multiplied by the given factors to implement all signals within one plot.

hydrogen was used as the purge gas during the TPD. Hence, partial pressures with by far the highest values are observed for mass m–4 for all samples. For all samples, the intensity of m–4 is more or less constant with a negative kink at about 400 °C (an exception is sample LT–7.5–LC_a that does not reveal such a kink). Hydrogen with mass m–2 shows mainly one broad peak starting at above 200 °C and ending above 1000 °C for all samples with maxima at about 590 °C; in some cases, this peak reveals shoulders. The mass m-3 can also be measured in considerable amounts and exhibits almost the same curve progression as m-4, but at lower partial pressures. At higher temperatures, m–3 slightly increases compared to m–4. Both masses can be assigned to two relevant species each: m-4 to He–4 and partially tritiated hydrogen (HT), as well as m-3 to tritium (T) and He–3. The latter is the decay product of tritium and about 38 % of the generated tritium is estimated to have decayed between the end of the HICU experiment and the start of the HICU PIE. No quantitative information can be derived about the gaseous species He–4, HT, T, and He–3, because it is not possible to distinguish them in the QMS signals. A release of T_2 with mass m–6 was not observed. A signal for m–6 was also not expected as it is unlikely that two single tritium atoms bond together compared to a reaction with the abundantly available molecules H_2 or H_2O. Blynskiy et al. observed the release of T_2 from Li_2TiO_3 in situ. As for HT, an increase in the T_2 release was shown with increased reactor power [31].

Another signal with a significant partial pressure is that of water (m–18). During the HICU experiment both irradiation temperatures were high enough to remove water from the pebbles. Hence, the water must have been adsorbed after the irradiation and during the storage of the samples. All but one sample show a constant release of water in the beginning of the TPD, with a more or less steeply increasing release from 200 °C and a flattening of the m–18-curve above ~500 °C. Again, the sample LT–7.5–LC_a exhibits a different curve progression for m–18. Here, the release curve is almost steadily rising up to ~825 °C and decreases afterwards. Moreover, the signals of water-related T–species are plotted in Fig. 14: m–19 (OT), m–20 (HTO) and m–22 (T_2O). Most signals are very low in intensity, but in all samples a peak at least slightly above the background noise can be observed for semi-tritiated water HTO (m–20) and its fragment OT (m–19). At approximately 450 °C, the peak maxima occur during the increase of the water (m–18) release. Both samples with a natural Li–6 abundance originating from the same batch exhibit signals of m–19 with higher (HT–7.5–LC) and significantly higher (LT–7.5–LC_a) intensities. While the curve progression for m–19 in HT–7.5–LC is similar to that of the other samples with a peak at about 440 °C, it is different again for sample LT–7.5–LC_a. In sample LT–7.5–LC_a, the curve of m–19 follows the progression of m–18, showing a peak at about 825 °C. Only in sample LT–7.5–LC_a is the relative intensity of m–20 slightly higher and shows a similar curve progression to m–18 and m–19. No signal for m–22 corresponding to tritiated water (T_2O) was observed in any sample. This is not astonishing as it is much more likely that an exchange reaction of tritium with H_2O happens compared to an exchange reaction with a previously formed HTO as the availability of water is much higher.

A relation between the specific release curves measured by IC and the release curves of gaseous species measured by QMS can hardly be observed. The specific release curves increase significantly at about 450 °C for all samples. The peaks of clearly T-related signals m–19 and m–20 are observed at about 430 °C and 460 °C for samples irradiated at high and low temperatures, respectively. Yet, there are no further peaks in the QMS signals following the peak maxima of the IC curves. Sample LT–7.5–LC_a exhibits peak maxima for m–19 and m–20 at about 825 °C and 810 °C, respectively, and the signal of m–19 is significantly higher compared to the other samples. However, the curve progression of masses does not match the peak temperature of the specific release curve

at about 865 °C.

4. Conclusions

The material properties of ten Li_2TiO_3 pebble samples that were irradiated with neutrons within the HICU experiment were investigated in this study.

It can be concluded, that the irradiation temperature has the most significant influence on the pebbles' behaviour and properties. A high irradiation temperature seems to be beneficial for the efficient release of tritium. Therefore, the formation of a secondary lithium-depleted phase appears to be enhanced on the surface of the pebbles at high temperatures.

Effects with respect to the initial Li–6 content seem to be low. The phase analyses show a slight trend for an increased formation of the lithium-depleted phase and thus more lithium was transmuted with a higher the Li–6 content. There is a tendency that the tritium inventory is lower with higher initial Li–6 content. However, it can only be assumed that the generated tritium could have been released more easily already during the irradiation due to a higher concentration gradient.

A constraint of the pebble bed does not have a significant effect on the material properties. Therefore, it is assumed that a compaction would not deteriorate the pebbles' properties.

The status of the microstructure cannot be directly compared with the pristine one. However, a moderate grain growth is observed. The closed porosity increased, which could lead to tritium trapping in the material. The mechanical strength of the pebbles was reduced, but the cooling probably leads to further cracks that would not occur at stable high temperatures. Tritium is released as HTO, HT and their respective fragments. Tritiated water T_2O and tritiated hydrogen T_2 are not detected as released species.

CRediT authorship contribution statement

Julia Leys: Writing – original draft, Visualization, Validation, Project administration, Methodology, Investigation, Conceptualization. **Rolf Rolli:** Writing – review & editing, Methodology, Investigation, Data curation. **Hans-Christian Schneider:** Writing – review & editing, Supervision, Resources. **Regina Knitter:** Writing – review & editing, Supervision, Funding acquisition, Conceptualization.

Declaration of competing interest

The authors declare that they have no known competing financial interests or personal relationships that could have appeared to influence the work reported in this paper.

Data availability

Data will be made available on request.

Acknowledgements

The authors greatly acknowledge the experimental support of Joachim Ehrmann, Sven Lautensack, Maik Rietschel, and Marco Weber in the fusion materials laboratory of KIT. This work has been carried out within the framework of the EUROfusion Consortium, funded by the European Union via the Euratom Research and Training Programme (Grant Agreement No 101052200 — EUROfusion). Views and opinions expressed are however those of the author(s) only and do not necessarily reflect those of the European Union or the European Commission. Neither the European Union nor the European Commission can be held responsible for them.

Appendix A. Supplementary data

Supplementary data to this article can be found online at https://doi.org/10.1016/j.nme.2024.101625.

References

[1] J.B.J. Hegeman, E.D.L. van Essen, M. Jong, J.G. van der Laan, J. Reimann, Thermomechanical behaviour of ceramic breeder pebble stacks for HICU, Fusion Eng. Des. 69 (2003) 425–429, https://doi.org/10.1016/S0920-3796(03)00086-3.
[2] M.H.H. Kolb, J.M. Heuser, R. Rolli, H.-C. Schneider, R. Knitter, M. Zmitko, The HICU PIE results of EU ceramic breeder pebbles: general characterization, J. Nucl. Mater. 531 (2020) 152023, https://doi.org/10.1016/j.jnucmat.2020.152023.
[3] J.M. Heuser, M.H.H. Kolb, R. Rolli, H.-C. Schneider, R. Knitter, M. Zmitko, The HICU PIE results of EU ceramic breeder pebbles: tritium release properties, J. Nucl. Mater. 531 (2020) 152024, https://doi.org/10.1016/j.jnucmat.2020.152024.
[4] J.D. Lulewicz, N. Roux, Fabrication of Li_2TiO_3 pebbles by the extrusion-spheronisation-sintering process, J. Nucl. Mater. 307–311 (2002) 803–806, https://doi.org/10.1016/S0022-3115(02)00981-9.
[5] K. Kataoka, Y. Takahashi, N. Kijima, H. Nagai, J. Akimoto, Y. Idemoto, K. Ohshima, Crystal growth and structure refinement of monoclinic Li_2TiO_3, Mater. Res. Bull. 44 (2009) 168–172, https://doi.org/10.1016/j.materresbull.2008.03.015.
[6] J.B.J. Hegeman, J.G. van der Laan, S. Kamer, S. de Groot, A high fluence irradiation of ceramic breeder materials in HFR Petten, test-matric and design of the irradiation, in: Proceedings of the 12th International Workshop on Ceramic Breeder Blanket Interactions, Karlsruhe, Germany, 2004.
[7] C.M. Sciolla, S.C. van der Marck, HICU (333-01) – Assessment of burn-up, dpa and nuclear heat, NRG note, ref. 20295/11.107312 LCI/CS/MK, 2011.
[8] Z. Li, J. Li, Y. Zhao, K. Yang, F. Gao, X. Li, Structure and electrochemical properties of sm-doped $Li_4Ti_5O_{12}$ as anode material for lithium-ion batteries, RSC Adv. 6 (2016) 15492–15500, https://doi.org/10.1039/C5RA27142H.
[9] M. Oyaidzu, Y. Morimoto, M. Sasaki, H. Kimura, K. Munakata, M. Nishikawa, K. Kawamoto, M. Okada, K. Okuno, ESR study on annihilation process of radiation defects induced in solid tritium breeding materials by neutron irradiation, Phys. Scripta 2004 (2004) 42–45, https://doi.org/10.1238/Physica.Topical.108a00042.
[10] S. Suzuki, M. Kobayashi, R. Kurata, W. Wang, T. Fujii, H. Yamana, K. Feng, Y. Oya, K. Okuno, Elucidation of annihilation processes of defects induced by γ-irradiation in Li_2TiO_3, Fusion Eng. Des. 85 (2010) 2331–2333, https://doi.org/10.1016/j.fusengdes.2010.09.022.
[11] J. Wang, Y. Xu, F. Liu, Z. An, T. Lu, M. Xiang, H. Zhou, X. Li, M. Zhao, Y. Zhang, G.-N. Luo, Q. Qi, Release behavior of hydrogen isotopes in deuterium-irradiated Li_2TiO_3, Fusion Eng. Des. 113 (2016) 318–323, https://doi.org/10.1016/j.fusengdes.2016.05.022.
[12] J. Osuo, M. Kobayashi, R. Kurata, A. Hamada, W. Wang, T. Fujii, H. Yamana, T. Luo, K. Feng, Y. Oya, K. Okuno, Dependence of gamma-ray dose on annihilation processes of irradiation defects in Li_2TiO_3, Fusion Eng. Des. 86 (2011) 2362–2364, https://doi.org/10.1016/j.fusengdes.2011.04.080.
[13] Q. Qi, J. Wang, M. Xiang, Y. Zhang, S. Gu, G.-N. Luo, Mechanism of vacuum-annealing defects and its effect on release behavior of hydrogen isotopes in Li_2TiO_3, Int. J. Hydrogen Energ. 43 (2018) 12295–12301, https://doi.org/10.1016/j.ijhydene.2018.05.050.
[14] J. Wang, Y. Xu, H. Liu, M. Xiang, H. Zhou, Y. Zhang, G.-N. Luo, Q. Qi, Influence of ion irradiations on the microstructure in the tritium breeder material Li_2TiO_3, Nucl. Instrum. Meth. B 450 (2019) 189–194, https://doi.org/10.1016/j.nimb.2018.04.013.
[15] D.L. Griscom, Electron spin resonance in glasses, J. Non-Cryst. Solids 40 (1980) 211–272, https://doi.org/10.1016/0022-3093(80)90105-2.
[16] T. Hoshino, H. Kawamura, M. Dokiya, Y. Takahashi, T. Terai, M. Yamawaki, Non-stoichiometry of Li_2TiO_3 under hydrogen atmosphere conditions, J. Nucl. Mater. 329–333 (2004) 1300–1304, https://doi.org/10.1016/j.jnucmat.2004.04.226.
[17] N. Nakashima, S. Beloglazov, K. Hashimoto, M. Nishikawa, Isotope exchange reaction between gaseous hydrogen and tritium on Li_2TiO_3 grain surface, Fusion Sci. Technol. 41 (2002) 1044–1048, https://doi.org/10.13182/FST02-A22743.
[18] H. Kleykamp, Phase equilibria in the li-ti-O system and physical properties of Li_2TiO_3, Fusion Eng. Des. 61–62 (2002) 361–366, https://doi.org/10.1016/S0920-3796(02)00120-5.
[19] T. Hoshino, M. Dokiya, T. Terai, Y. Takahashi, M. Yamawaki, Non-stoichiometry and its effect on thermal properties of Li_2TiO_3, Fusion Eng. Des. 61–62 (2002) 353–360, https://doi.org/10.1016/S0920-3796(02)00216-8.
[20] T. Hoshino, M. Yasumoto, K. Tsuchiya, K. Hayashi, H. Nishimura, A. Suzuki, T. Terai, Vapor species evolved from Li_2TiO_3 heated at high temperature under various conditions, Fusion Eng. Des. 81 (2006) 555–559, https://doi.org/10.1016/j.fusengdes.2005.10.004.
[21] A. Lecerf, Sur quelques proprietes chimiques des oxydes TiO et Ti_2O_3-preparation et etudes de nouveaux composes ternaires oxygenes du titane trivalent, Ann. Chim. France 7 (1962) 513.
[22] R.D. Shannon, Revised effective ionic radii and systematic studies of interatomic distances in halides and chalcogenides, Acta Crystallogr. A 32 (1976) 751–767, https://doi.org/10.1107/S0567739476001551.
[23] S. van Til, A.V. Fedorov, A.J. Magielsen, Study of ceramic pebble beds in post irradiation examination of the pebble bed assemblies irradiation experiment, Fusion Eng. Des. 87 (2012) 885–889, https://doi.org/10.1016/j.fusengdes.2012.02.052.

[24] G. Piazza, J. Reimann, E. Günther, R. Knitter, N. Roux, J.D. Lulewicz, Behaviour of ceramic breeder materials in long time annealing experiments, Fusion Eng. Des. 58–59 (2001) 653–659, https://doi.org/10.1016/S0920-3796(01)00517-8.
[25] Y. Otani, K. Shin-mura, S. Ogawa, T. Hoshino, K. Sasaki, Changes in mechanical property and microstructure of lithium metatitanate tritium breeder caused by thermal annealing, Fusion Eng. Des. 124 (2017) 801–804, https://doi.org/10.1016/j.fusengdes.2017.03.158.
[26] K. Mukai, M. Yasumoto, T. Terai, Lithium vapor chemistry of hyper-stoichiometric lithium metatitanate Li2.12(2)TiO3+y, J. Phys. Chem. C 124 (2020) 10870–10877, https://doi.org/10.1021/acs.jpcc.0c02454.
[27] H. Hamilton, The thermal cycling behaviour of lithium titanate, J. Nucl. Mater. 219 (1995) 274–283, https://doi.org/10.1016/0022-3115(94)00402-1.
[28] S. van Til, A.J. Magielsen, M.P. Stijkel, H.L. Cobussen, Out of pile tritium release behaviour and microscopic investigation of lithium metatitanate irradiated in the high flux reactor in petten, Fusion Eng. Des. 85 (2010) 1143–1146, https://doi.org/10.1016/j.fusengdes.2010.02.022.
[29] T. Kinjyo, M. Nishikawa, M. Enoeda, S. Fukada, Tritium diffusivity in crystal grain of Li_2TiO_3 and tritium release behavior under several purge gas conditions, Fusion Eng. Des. 83 (2008) 580–587, https://doi.org/10.1016/j.fusengdes.2007.11.011.
[30] M. Yang, L. Zhao, G. Ran, Y. Gong, H. Wang, S. Peng, C. Xiao, X. Chen, T. Lu, Tritium release behavior of Li_2TiO_3 and $2Li_2TiO_3$-Li_4SiO_4 biphasic ceramic pebbles fabricated by microwave sintering, Fusion Eng. Des. 168 (2021) 112390, https://doi.org/10.1016/j.fusengdes.2021.112390.
[31] P. Blynskiy, Y. Chikhray, T. Kulsartov, M. Gabdullin, Z.h. Zaurbekova, G. Kizane, Y. Kenzhin, A. Tolenova, E. Nesterov, A. Shaimerdenov, Experiments on tritium generation and yield from lithium ceramics during neutron irradiation, Int. J. Hydrogen Energ. 46 (2021) 9186–9192, https://doi.org/10.1016/j.ijhydene.2020.12.224.